AGU PUBLICATIONS

JGR

Journal of Geophysical Research: Atmospheres

RESEARCH ARTICLE
10.1002/2015JD023438

Special Section:
East Asian Study of Tropospheric Aerosols and Impact on Cloud and Precipitation

Key Points:
- Microwave radiometer retrieved temperature, vapor density, and RH accuracies
- Compare MWR retrievals and radiosonde measurements under clear and cloudy skies
- MWR retrieval accuracies under low, middle, and high clouds identified by IRT

Correspondence to:
B. Xi,
baike@aero.und.edu

Citation:
Xu, G., B. Xi, W. Zhang, C. Cui, X. Dong, Y. Liu, and G. Yan (2015), Comparison of atmospheric profiles between microwave radiometer retrievals and radiosonde soundings, *J. Geophys. Res. Atmos.*, *120*, doi:10.1002/2015JD023438.

Received 26 MAR 2015
Accepted 9 SEP 2015
Accepted article online 14 SEP 2015

Comparison of atmospheric profiles between microwave radiometer retrievals and radiosonde soundings

Guirong Xu[1], Baike Xi[2], Wengang Zhang[1], Chunguang Cui[1], Xiquan Dong[1,2,3], Yuanyuan Liu[4], and Guopao Yan[5]

[1]Hubei Key Laboratory for Heavy Rain Monitoring and Warning Research, Institute of Heavy Rain, China Meteorological Administration, Wuhan, China, [2]Department of Atmospheric Sciences, University of North Dakota, Grand Forks, North Dakota, USA, [3]College of Global Change and Earth System Science, Beijing Normal University, Beijing, China, [4]Hubei Meteorological Information and Technological Support Center, Wuhan, China, [5]Wuhan Meteorological Bureau of Hubei Province, Wuhan, China

Abstract Atmospheric profiles of temperature (T), vapor density (ρ_v), and relative humidity (RH) retrieved from ground-based microwave radiometer (MWR) measurements are compared with radiosonde soundings at Wuhan, China. The MWR retrievals were averaged in the ±30 min period centered at sounding times of 00 and 12 UTC. A total of 403 and 760 profiles under clear and cloudy skies were selected. Based on the comparisons, temperature profiles have better consistency than the ρ_v and RH profiles, lower levels are better than upper levels, and the cloudy are better than the clear-sky profiles. Three cloud types (low, middle, and high) were identified by matching the infrared radiation thermometer-detected cloud base temperature to the MWR-retrieved temperature-height profiles. Temperature profile under high cloud has the highest correlation coefficient (R) and the lowest bias and RMS, but under low cloud is in the opposite direction. The ρ_v profile under middle cloud has the highest R and the lowest bias but under high cloud has the lowest R, the largest bias, and RMS. Based on the radiosonde soundings, both clear and cloudy wind speeds and drifting distances increase with height but increase much faster under clear than cloudy above 4 km. The increased wind speeds and drifting distances with height have resulted in decreased correlation coefficient and increased temperature biases and RMSs with height for both clear and cloudy skies. The differences in R, bias, and RMS between clear and cloudy skies are primarily resulted from their wind speeds and drifting distances.

1. Introduction

Atmospheric water vapor is the most important greenhouse gas in manipulating the Earth radiation budgets and plays a very crucial role in meteorological, hydrological, and climate systems [*Starr and Melfi*, 1991]. Numerous efforts have been made to understand the horizontal and vertical distributions of water vapor. A few sophisticated techniques have been developed to measure the water vapor from ground-based observations, such as the radiosonde and microwave radiometer (MWR). MWR is a typical passive remote sensing device and measures brightness temperatures at the frequencies of 22–30 GHz and 51–59 GHz approximately every 3 min. The brightness temperatures measured by the MWR can be used to retrieve the atmospheric column-integrated water vapor (PWV) and liquid water path (LWP) using a statistical method [*Liljegren et al.,* 2001].

The advantage of the method is simple and relatively accurate because the relationships between the opacities and the retrieved PWV and LWP are determined by linear regressions. However, the disadvantage is that the method needs a large prior data set at specific locations for getting representative retrieval coefficients [*Liljegren et al*., 2001]. The data sets used in the method are usually from radiosonde soundings. One limitation of the method is when moderate and heavy precipitation events happen, the PWV and LWP retrievals become unreliable due to contamination of rainwater on the sensor covering [*Morris et al.,* 2006]. The retrieval coefficients are calculated using previous monthly data from the site to account for variations in the underlying parameters over the course of an annual cycle. Although the radiosonde can provide the fundamental measurements of atmospheric temperature in addition to wind and water vapor profiling, twice-daily radiosonde data are inadequate for the detection of mesoscale phenomena.

The MWR measures the atmospheric brightness temperature at different frequencies, which is influenced by atmospheric temperature, humidity, and the presence of hydrometeors. From calibrated brightness

temperature, the MWR can retrieve temperature, humidity, and liquid profiles up to 10 km at temporal resolutions of 0.5 to 5 min [*Solheim et al.,* 1998; *Ware et al.,* 2003; *Löhnert et al.,* 2004; *Cimini et al.,* 2006; *Chan*, 2009]. These profiles are available nearly continuously and can be very useful for the detection of mesoscale phenomena that require very high spatial and temporal scales [*Knupp et al.,* 2009; *Madhulatha et al.,* 2013; *Harikishan et al.,* 2014]. The accuracy of MWR profiles is compatible with most meteorology applications, especially in the lower troposphere [*Güldner and Spänkuch*, 2001; *Hewison*, 2007; *Chan and Hon*, 2011; *Cimini et al.,* 2011; *Ware et al.,* 2013].

The MWR has become a popular and efficient instrument for remotely sensing the atmospheric temperature and humidity profiles as well as path-integrated cloud liquid water content in last few decades. MWRs are operated in many countries for monitoring climate and meteorological phenomena (e.g., nowcasting convective activity, boundary layer meteorology, and clouds) [*Spänkuch et al.,* 2011; *Xie et al.,* 2011; *Cimini et al.,* 2013; *Cadeddu et al.,* 2013; *Madhulatha et al.,* 2013; *Raju et al.,* 2013; *Venkat Ratnam et al.,* 2013; *Ware et al.,* 2013; *Calheiros and Machado*, 2014; *Campos et al.,* 2014; *Clements and Oliphant*, 2014; *Serke et al.,* 2014; *Xu et al.,* 2014; *Gultepe et al.,* 2015].

The retrieval method normally does not take the scattering and emission/absorption effects of rain into account. Compared to radiosonde observations, the bias and root-mean-square (RMS) of MWR retrievals under precipitation are not as small as those during nonprecipitation conditions [*Xu et al.,* 2014]. Note that the nonprecipitation conditions include clear and cloudy skies, yet few studies report the discrepancies of MWR retrievals against radiosonde soundings under clear and cloudy skies. In this study, we investigate the discrepancies of MWR retrievals under clear and cloudy skies using collocated radiosonde soundings as a ground truth. This paper is organized as follows: Section 2 will briefly describe the instruments, measurements, and retrieval method; section 3 compares the MWR-retrieved atmospheric profiles of temperature and humidity with collocated radiosonde soundings over Wuhan, China, and discusses the accuracies of MWR retrievals under clear and cloudy skies; and section 4 summarizes our findings.

2. Data and Methodology

An operational weather station is located at Wuhan, China (30.6°N, 114.1°E, 23 m above sea level). The radiosonde releases twice daily at 00 and 12 UTC and can provide atmospheric temperature and humidity profiles, and the wind speed and direction. A Radiometrics MP-3000A MWR has been in operation at this station since June 2010. This particular MWR observes atmospheric brightness temperatures with a total of 21 K-band (22–30 GHz) and 14 V-band (51–59 GHz) microwave channels at multiple elevation angles, and atmospheric background or cloud base temperatures at one zenith infrared (9.6–10.5 μm) channel [*Cimini et al.,* 2011; *Ware et al.,* 2013].

To minimize the measurement errors caused by precipitation on the MWR antenna radome, which is made of hydrophobic material that is transparent to radio waves, a special blower system is used to sweep water beads and snow away from the radome [*Chan*, 2009]. A rain sensor equipped with the MWR is used to provide a "Rain Flag," which senses whether any liquid water covers the radome during heavy rain events. A Rain Flag of zero (Rain = 0) represents nonprecipitation and a value of one (Rain = 1) represents precipitation conditions. A zenith-looking infrared radiation thermometer (IRT) on the MWR is used to measure atmospheric background temperature during clear sky and the cloud base temperature during cloudy condition. The cloud base height (CBH) can then be set to the lowest height where the cloud base temperature from IRT is equal to the MWR-retrieved temperature profile [*Ware et al.,* 2003]. Clear sky can be distinguished from cloudy (liquid or ice) sky by the IRT because atmospheric background temperature is lower than ice cloud base temperature, and much lower than liquid cloud base temperature. If cloud is detected by the IRT and the MWR-retrieved cloud liquid water path (LWP) is around zero, ice cloud can be deduced. Therefore, the sky condition can be determined by both the IRT and MWR. A CBH value equal to −1 indicates no CBH (i.e., clear sky), CBH equal to 0 means fog or precipitation conditions, and CBH greater than 0 denotes cloudy sky.

The temperature (T), relative humidity (RH), and vapor density (ρ_v) profiles in this study are retrieved from MWR measurements at zenith direction. The retrieved algorithm developed by the factory can automatically convert the microwave, infrared, and surface meteorological measurements into temperature, humidity, and liquid profiles using radiative transfer equations with the aid of neural networks. Five years of historical Wuhan radiosondes (downloaded from http://esrl.noaa.gov/raobs) were used to train the neural networks [*Durre et al.*, 2008].

Four vector neural networks including 26 inputs (8 K-band, 14 V-band microwave channels, an infrared channel, and 3 surface meteorological channels) and 49 hidden nodes generate 58 output nodes (temperature, relative humidity, liquid density, and vapor density retrieval heights). Scalar neural networks use the same input and hidden nodes to generate integrated atmospheric precipitable water vapor (PWV) and LWP outputs [*Ware et al.,* 2013]. This iteration process will be stopped when the neural network training change is less than 0.1%.

The temperature, humidity, and liquid profiles retrieved from MWR observations have a temporal resolution of 3 min, and vertical resolutions of 50 m from the surface to 500 m, 100 m from 500 m to 2 km, and 250 m from 2 km to 10 km [*Ware et al.,* 2013; *Xu et al.,* 2014]. Background error covariance analysis shows that retrieval information for both temperature and water vapor is highest near ground level, decreases with height, and is limited above 1 km [*Cimini et al.,* 2011; *Ware et al.,* 2013]. The comparisons between the radiosonde soundings and MWR retrievals from previous studies demonstrate that accuracies of MWR temperature and humidity retrievals are equivalent to measurement error assigned to radiosonde soundings during assimilation in numerical weather models [*Güldner and Spänkuch*, 2001].

A ceilometer made by China Huayun Corporation started to operate at Wuhan since December 2012, which can provide continuous CBHs at a 1 min temporal resolution. For this study, the ceilometer-derived CBHs during the period December 2012 to December 2013 have been collected and used for validating the IRT-inferred CBHs. There are a total of 3032 matched samples (1 min) between the ceilometer and IRT measurements under cloudy conditions with a correlation coefficient of 0.56 and a system bias of −0.55 km. For different levels of clouds, the CBH biases (IRT-ceilometer) are −0.84, −0.50, and 1.32 km, respectively, for low (CBH < 2 km), middle (2 km ≤ CBH ≤ 7 km), and high (CBH > 7 km) clouds. Note that the uncertainties of ceilometer-derived CBHs are ±10% below 1 km and ±20% above 1 km. The negative biases of IRT CBHs for low and middle clouds are likely due to the uncertainties of ceilometer observations and IRT retrievals, while for high clouds, the positive bias is most likely due to the upper limit of 7.5 km in ceilometer observations. Based on the comparisons of CBHs between ceilometer and IRT, we think that the IRT-inferred CBHs are reasonable in this study.

The radiosondes (launched twice daily: 00 and 12 UTC) used in this study are L-band radio sounding systems, providing vertical pressure, temperature, relative humidity, dew point temperature, and wind profiles at a 1 s temporal resolution. The radiosonde profiles from June 2010 to December 2013 have been collected and used for validating the MWR-retrieved temperature and humidity profiles. The MWR is calibrated by using liquid nitrogen in a top mount target in the beginning of each season, and the calibration accuracy is within 0.5°C.

Based on the IRT-inferred CBHs, only the MWR profiles under clear (CBH = −1) and cloudy (CBH > 0) skies are selected in this study (Figure 1g). Since the radiosondes are launched at 00 and 12 UTC, the MWR profiles are averaged over a 1 h interval centered at 00 and 12 UTC, and the averaged MWR profiles are compared with the corresponding radiosonde soundings (Figure 1).

Figure 1b shows four temperature profiles retrieved by the MWR and measured by radiosonde under clear and cloudy skies. The two temperature profiles under clear sky (2 red lines) agree within ~1°C below 2 km, and deviate above ~4 km. The temperature profiles under cloudy sky agree well up to ~7.5 km and then start to depart each other. Compared to the radiosonde-measured temperature profiles, the MWR retrievals cannot capture the temperature inversions due to the coarse vertical resolutions from limited weighting functions, particularly at upper levels. The vapor density and RH profiles under clear sky shown in Figures 1d and 1f agree well with soundings under ~1 km, and the differences become large above 1 km. Under cloudy-sky condition, both MWR-retrieved and radiosonde-measured vapor density and RH increase significantly from CBH (~2 km), maintain high within cloud layer and decrease dramatically at cloud top (~5 km) although there are slight differences between two profiles.

These comparisons are encouraging. Therefore, we will provide some statistical comparisons between the MWR retrievals and radiosonde soundings using long-term observations in this study. Based on available CBHs from IRT, we will further investigate the MWR retrievals under low, middle, and high clouds. The low clouds are defined as CBH < 2 km, middle clouds as 2 km ≤ CBH ≤ 7 km, and high clouds as CBH > 7 km. The MWR retrievals for three levels of clouds are also processed and compared with radiosonde soundings, following the steps in Figure 1.

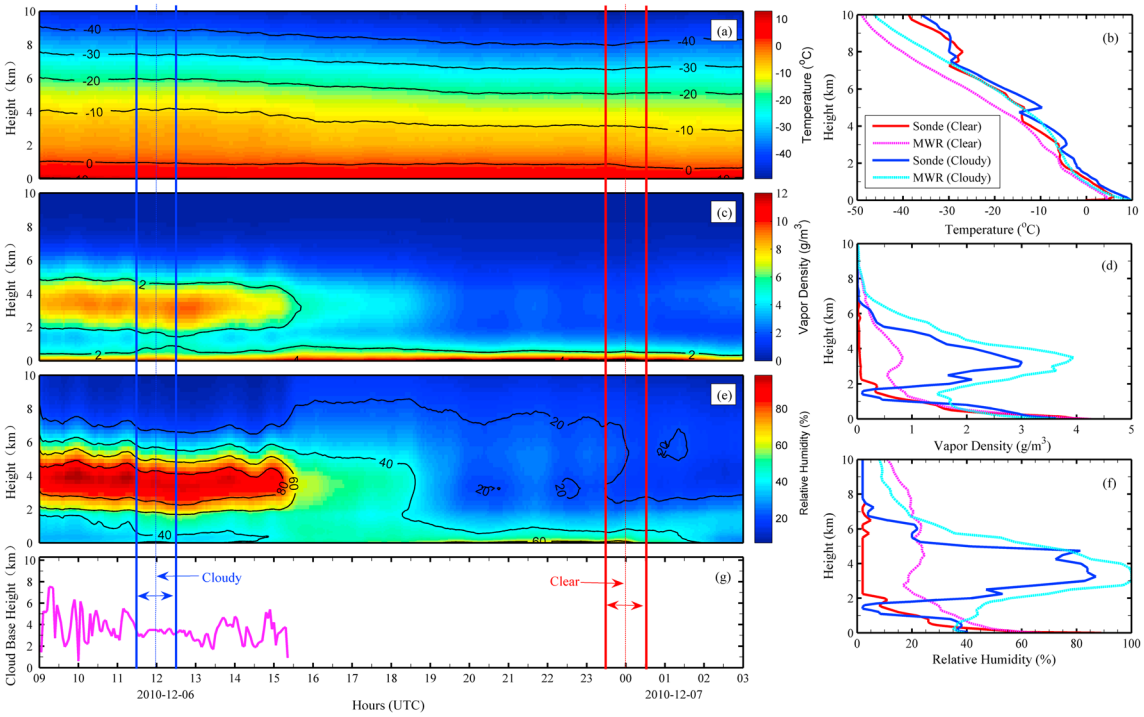

Figure 1. A schematic diagram illustrates the selection of cloudy and clear periods for comparison between radiosonde profiles and MWR retrievals. Three blue (red) vertical lines represent the ±30 min cloudy (clear) period centered at the sounding time of 12 (00) UTC. The MWR-retrieved (a) temperature, (c) vapor density, and (e) relative humidity profiles are first averaged in a 1 h interval centered at the sounding time and then compared with the corresponding radiosonde measured (b) temperature, (d) vapor density, and (f) relative humidity profiles. (g) Sky conditions are separated into clear and cloudy skies with the cloud base height derived from IRT equipped on MWR.

Methods used in this study are simply and straightforward, and the correlation coefficients, biases, and RMSs between the MWR retrievals and the radiosonde measurements for each parameter (e.g., T, ρ_v, and RH) under different sky conditions and different cloud types are calculated. The discrepancies between MWR retrievals and radiosonde measurements at different heights are calculated to explore how the MWR retrievals vary with height. Finally, the impact of wind speeds and drifting distances on the comparisons is examined in-depth.

3. Results and Discussions

3.1. Uncertainties of MWR-Retrieved Atmospheric Profiles Under Clear and Cloudy Skies

A total of 403 radiosonde soundings under clear sky and 760 soundings under cloudy sky during the period June 2010 to December 2013 have been selected to assess the MWR-retrieved atmospheric profiles. Comparisons between radiosonde soundings and MWR retrievals during both clear-sky and cloudy conditions, and associated statistical results, are presented in Figure 2. For temperature comparisons, their correlation coefficients are greater than 0.85 from the surface up to ~7 km for both clear and cloudy skies but decrease sharply to 0.35 from ~7 km to 10 km for clear sky (Figure 2a). Compared to the radiosonde-measured temperatures, the MWR-retrieved temperatures have negative biases for both clear and cloudy skies (Figure 2b). The cloudy temperature biases are within −2°C below 7 km and then increase to −3°C at ~10 km, consistent to their correlation coefficients, whereas the clear-sky temperature biases increase from −2°C at 2 km to −6.5°C at 9 km. The RMSs for both clear and cloudy skies monotonically increase from 1°C at the surface to ~ 5°C at ~ 10 km with slightly large clear-sky RMSs at upper levels.

The atmospheric water vapor comparisons presented in Figures 2d–2f mimic their temperature comparisons, and the cloudy comparisons outperform the clear-sky comparisons. The correlation coefficients for cloudy sky decrease linearly from 1 at the surface to 0.5 at 10 km, while those for clear sky are even worse, down to 0.2 at 10 km. The dry biases at boundary layer for both clear and cloudy skies change to the wet biases

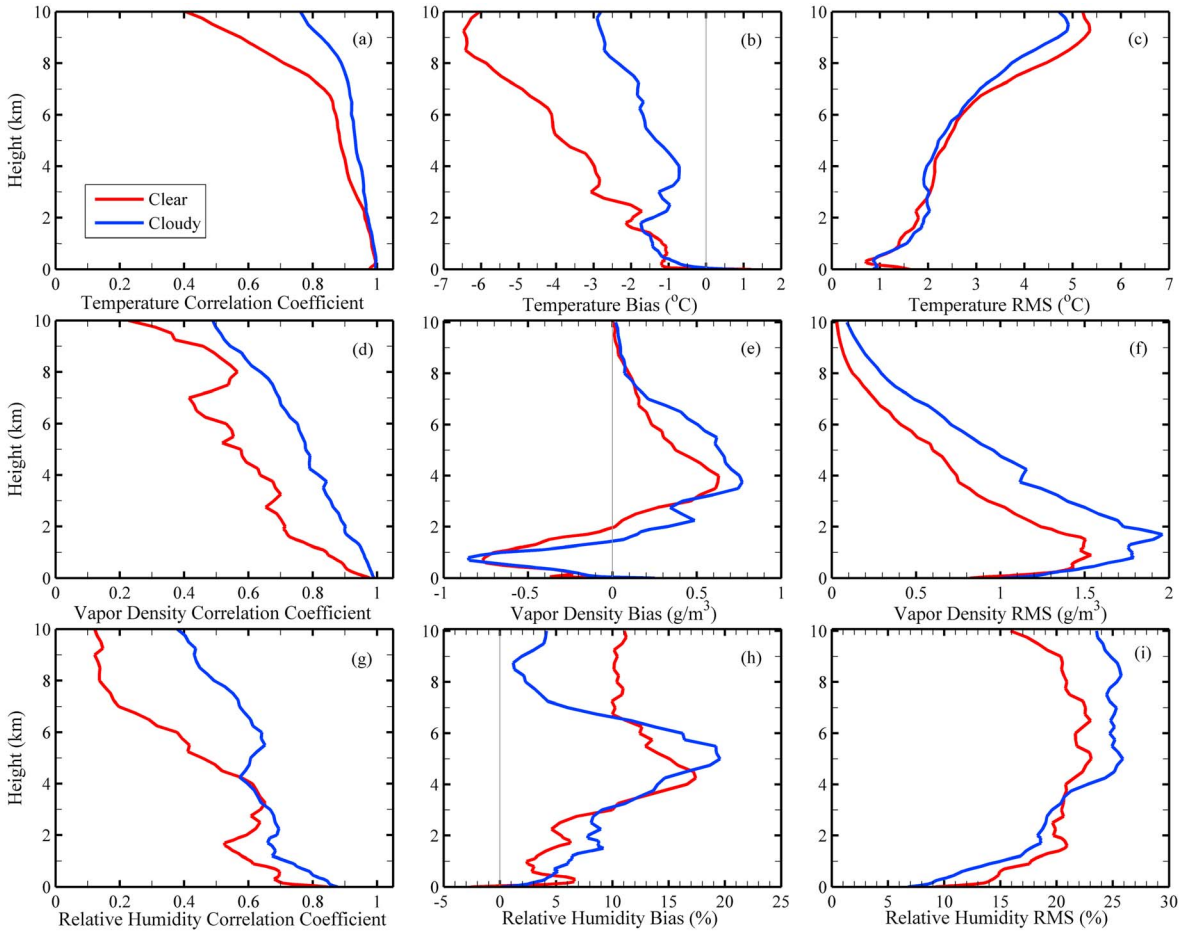

Figure 2. The correlation coefficients, biases, and RMSs of MWR-retrieved (a–c) temperature, (d–f) vapor density, and (g–i) relative humidity against radiosondes under clear (red lines) and cloudy (blue lines) skies. A total of 403 clear-sky profiles and 760 cloudy-sky profiles were selected from June 2010 to December 2013.

above 2 km with peaks of ~ 0.6 g m^{-3} at ~ 4 km. Note that the wet biases of cloudy sky are relatively larger than those of clear sky due to its higher water vapor characteristics. As a result, the RMS values of cloudy sky are consistently higher than those of clear sky from the surface to 10 km (Figure 2f).

The correlation coefficients of RHs for clear and cloudy skies are similar to their corresponding water vapor coefficients, decreasing monotonically with height but less than 0.8 (Figure 2g). Both clear and cloudy RH biases increase from ~ 3% at the surface to ~ 15–20% at 4–5 km and then decrease with height. The cloudy RH biases decrease significantly down to 1% at 9 km, while the clear-sky RH biases remain nearly invariant ~10% from 7 km to 10 km. Contradicting to the variations of water vapor, the RMS values of RH shown in Figure 2i increase with height monotonically up to ~2 km and 5 km under clear and cloudy skies, respectively, and then slightly vary around 20% for clear sky and 25% for cloudy sky.

Based on the comparisons in Figure 2, we can draw the following three conclusions: the temperature comparisons are better than the water vapor and RH ones; the comparisons at lower levels are better than those at upper levels; and the cloudy comparisons are better than the clear-sky ones. For the MWR-retrieved temperature profiles, 14 V-band (51–59 GHz) observations are input to the neural networks with more weighting functions at lower levels which results in finer vertical resolution of MWR retrievals at lower levels than at upper levels. For the water vapor density retrievals, only eight K-band (21–30 GHz) observations are input to the neural networks. Thus, their correlation coefficients are lower, and their biases and RMS values are larger than those of temperature. Since the MWR RH values are derived from the MWR-retrieved temperature and water vapor density, it is obvious that their correlation coefficients are lower, and their biases and RMS values are larger than those of temperature and water vapor density.

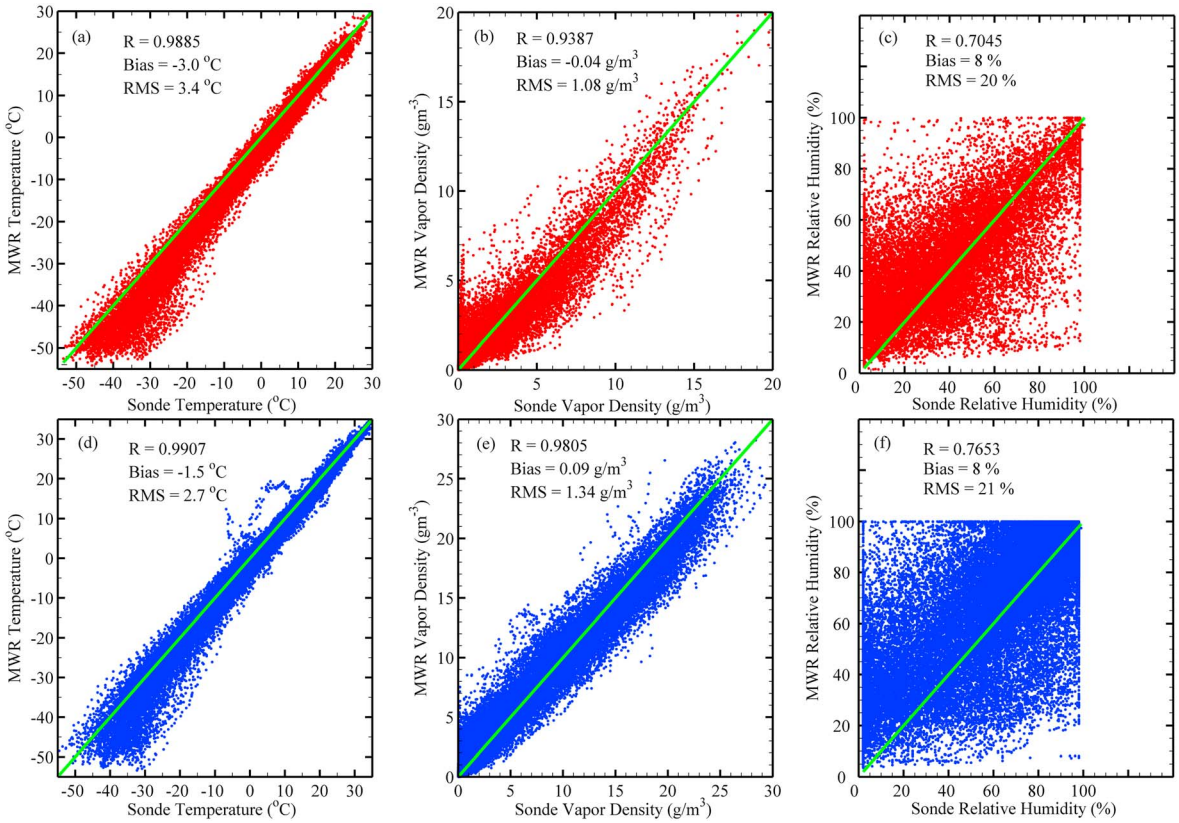

Figure 3. Scatterplots for MWR-retrieved (a, d) temperature, (b, e) vapor density, and (c, f) relative humidity against radiosondes under clear (Figures 3a–3c, red dots) and cloudy (Figures 3d–3f, blue dots) skies. There are a total of 23,374 and 44,080 matched samples under clear and cloudy skies, respectively, from June 2010 to December 2013.

It is well known that radiosonde humidity has systematic dry bias relative to the Cryogenic Frostpoint Hygrometer while the temperature has positive bias from solar heating [*Vömel et al.,* 2007; *Yoneyama et al.,* 2008; *Bian et al.,* 2011]. The MWR temperature biases against radiosondes shown in Figure 2b are negative under both clear and cloudy skies and increase with height, but the cloudy temperature biases are much smaller than the clear-sky ones above 2 km, presumably due to less solar heating on the radiosonde sensors. For clear sky, there are more solar heating on the radiosonde sensors, resulting in large positive biases in radiosonde temperature measurements. Therefore, we conclude that the linearly increased negative temperature biases with height during clear sky are most likely due to the strong solar heating on the radiosonde sensors at upper levels. In contrast to positive bias in the radiosonde temperature measurements, there is a dry bias in the water vapor measurements, which possibly results in the positive biases in the MWR-retrieved water vapor and RH for both clear and cloudy skies.

Figure 3 presents the scatterplots for MWR retrievals against radiosonde measurements with a total of 23,374 and 44,080 matched samples under clear and cloudy skies, respectively, from June 2010 to December 2013. Figure 3a shows the clear-sky temperature comparison with a correlation coefficient of 0.98, a bias of −3.0°C and an RMS of −3.4°C, while Figure 3d illustrates the cloudy temperature comparison with a slight higher correlation coefficient of 0.99, and lower bias of −1.5°C and RMS of −2.7°C. These comparisons are consistent with those in Figure 2, that is, the cloudy temperatures retrieved from MWR agree with the radiosonde measurements better than the clear-sky ones. The water vapor comparisons are slightly different to the temperature ones as shown in Figures 3b and 3e. Although the correlation coefficient is higher during cloudy sky than during clear sky, the cloudy water vapor bias and RMS are larger than the corresponding clear-sky ones due to the characteristic of much higher water vapor during cloudy conditions as discussed in Figure 2. As expected, the RH comparisons are much worse than the temperature and water vapor ones because they derived from the temperature and water vapor.

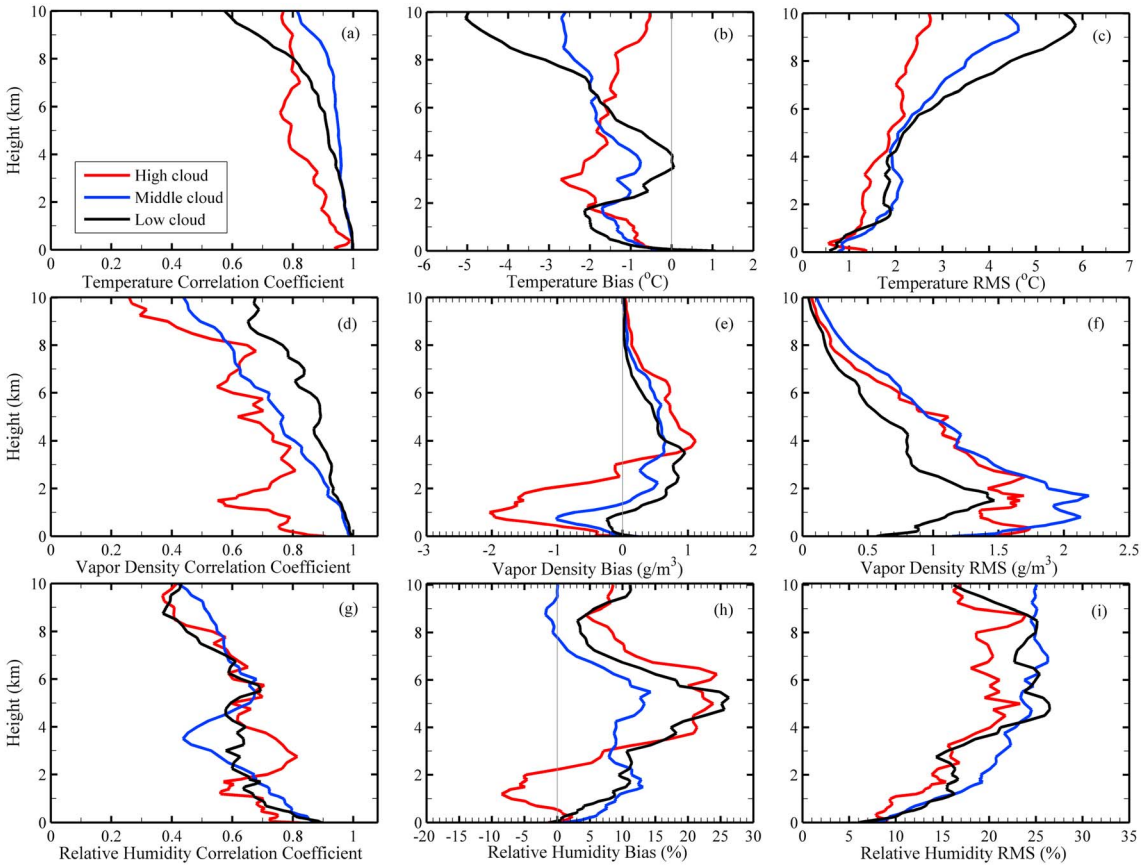

Figure 4. The correlation coefficients, biases, and RMSs of MWR retrieved (a–c) temperature, (d–f) vapor density, and (g–i) relative humidity against radiosondes under low (black lines), middle (blue lines), and high (red lines) clouds. The selected profiles from June 2010 to December 2013 under low, middle, and high clouds are 139, 274, and 47, respectively.

3.2. Uncertainties of MWR-Retrieved Atmospheric Profiles Under Three Types of Clouds

Matching the IRT-measured cloud base temperatures to the MWR-retrieved temperature profiles, we can identify and classified clouds into three types (low, middle, and high) with 139, 274, and 47 collocated radiosonde soundings. It is important to note that the sum of profiles (460) by these three types of clouds is much less than the number of the total cloudy profiles (760) because the profiles that have mixed cloud types are excluded. In other words, all profiles in this section should have a relatively uniformed CBH for each type. As mentioned above, the definitions of low, middle, and high clouds are CBH $<$ 2 km, 2 km $\leq$ CBH $\leq$ 7 km and CBH $>$ 7 km, respectively. Strictly speaking, these definitions are different from previous studies [*Dong et al.,* 2006; *Xi et al.,* 2010]; however, there are no cloud top measurements so far. Therefore, the current analyses can only guarantee no clouds below 2 km for middle clouds and no clouds below 7 km for high clouds, while for low clouds they can be either single layer or multilayer clouds.

Figure 4 is similar to Figure 2 except for three types of clouds. The temperature correlation coefficients shown in Figure 4a are the highest for middle cloud with values greater than 0.8 and the lowest for high cloud below 8 km, while low cloud has the lowest correlation coefficients above 8 km. Figure 4b indicates that the temperature biases are negative except near surface with positive biases within 1°C. The negative biases of low cloud range from 0°C at 2–5 km to −5.1°C at 10 km, while the negative biases of middle and high clouds vary from −0.5°C to −2.7°C. The temperature RMSs of low, middle, and high clouds are close to each other below 6 km (Figure 4c), while above 6 km they are the largest for low cloud and the smallest for high cloud, and their maximum RMSs are 5.9, 4.6, and 2.8°C, respectively.

Figures 4d–4f present statistics for the water vapor density. The correlation coefficients are generally highest for low cloud and lowest for high cloud, their biases change from negative at lower levels to positive at upper

levels, and the RMSs increase from the surface to ~2 km and then decrease with height. The peak negative biases for low, middle, and high clouds are −0.25, −1.01, and −2.05 g/m^3 at lower levels, while the positive biases at upper levels have insignificant differences with the peak values of 0.96, 0.66, and 1.12 g/m^3, respectively. In general, the RMSs are the smallest under low cloud and the largest under middle cloud, and the maximum RMSs for low, middle, and high clouds are 1.47, 2.19, and 1.74 g/m^3, respectively.

As shown in Figure 4g, the correlation coefficients of RHs for three types of clouds are similar to each other, less than 0.8 except near the surface and at 2–4 km the correlation coefficients of RHs are the lowest for middle cloud and the highest for high cloud. The biases of RH shown in Figure 4h are mostly positive and peak at ~5 km except negative above 8 km under middle cloud and below 2 km under high cloud. The maximum positive biases of RH for low, middle, and high clouds are 26%, 14%, and 24%, respectively. In general, the biases of RH are the smallest for middle cloud and the largest for high cloud. Figure 4i indicates that the RMSs of RH increase with height monotonically up to 5 km and then stay almost constant above their peaks except a decrease above 8.5 km for low and middle clouds. The RMSs of RH are the smallest for high cloud and the largest for middle cloud, and the peaks for low, middle, and high clouds are 26%, 26%, and 24%, respectively.

The scatterplots for MWR retrievals against radiosonde soundings under low, middle, and high clouds are presented in Figure 5. There are a total of 8062, 15,892, and 2726 matched samples under low, middle, and high clouds from June 2010 to December 2013, respectively. For temperature, high cloud has the highest correlation coefficient and the lowest bias and RMS, but low cloud is in the opposite direction. For water vapor density, middle cloud has the highest correlation and the lowest bias, and high cloud has the lowest correlation coefficient and the largest bias and RMS. This is understandable because high cloud has little liquid water and the noise level of the MWR measurements is relatively high; thus, the MWR has difficult to discern noise signal from the MWR measurements when the liquid content is very low. As mentioned above, the current analyses can only guarantee no clouds below 2 km for middle cloud and no clouds below 7 km for high cloud. A further work to explore this issue with additional ground-based and satellite-based observations is warranted. For RH comparisons, they are derived from both temperature and water vapor as discussed in Figures 2 and 3.

Table 1 summarizes the contribution of each cloud type to the total clouds. The correlations coefficients of temperature and vapor density are much higher than those of RHs, and the correlation, bias, and RMS of three parameters from middle cloud are close to those of total cloud. The dry bias from high cloud and wet bias from low cloud for vapor density are in similar order of magnitude, and their contributions to the total cloud bias are canceled out. The separation of the cloud types does not help us understand the impact of clouds on the uncertainties of MWR retrievals significantly due to lack of the cloud top measurements. With additional cloud top measurements, we can more accurately classify the cloud types and have better information about the performance of the MWR for different types of clouds.

3.3. Impact of Wind Speed on MWR Retrievals

Since the MWR retrievals (directly above the surface site) and radiosonde soundings (drifting with wind) may be different, it is necessary to explore whether the biases between MWR retrievals and radiosonde sounding measurements associate with wind speed. Figure 6 illustrates the variations of radiosonde balloon drifting distance and wind speed along height based on a total of 23,374 clear-sky samples and 44,080 cloudy samples. The wind speeds monotonically increase with height for clear and cloudy skies below 3.5 km but then start to deviate after that. The wind speeds under clear sky increase from 10 m/s at a height of 4 km to 52 m/s at a height of 10 km, while those for cloudy sky only increase to 33 m/s at a height of 10 km. As a result, the drifting distances for cloudy sky increase from 4 km at a height of 4 km to 22 km at a height of 10 km; however, the maximum drifting distance for clear sky is 32 km at a height of 10 km. Based on the results in Figure 6, we can conclude that both clear and cloudy wind speeds increase with height, but clear sky wind speeds increase much faster than cloudy ones above 4 km, and the radiosondes drifting distance is strongly associated with wind speed.

Combining the findings in Figure 6 with those in Figure 2, we can conclude that the decreased correlation coefficients and increased temperature biases and RMSs with height for both clear and cloudy skies are strongly associated with the increased wind speeds and drifted distances. The differences in correlation

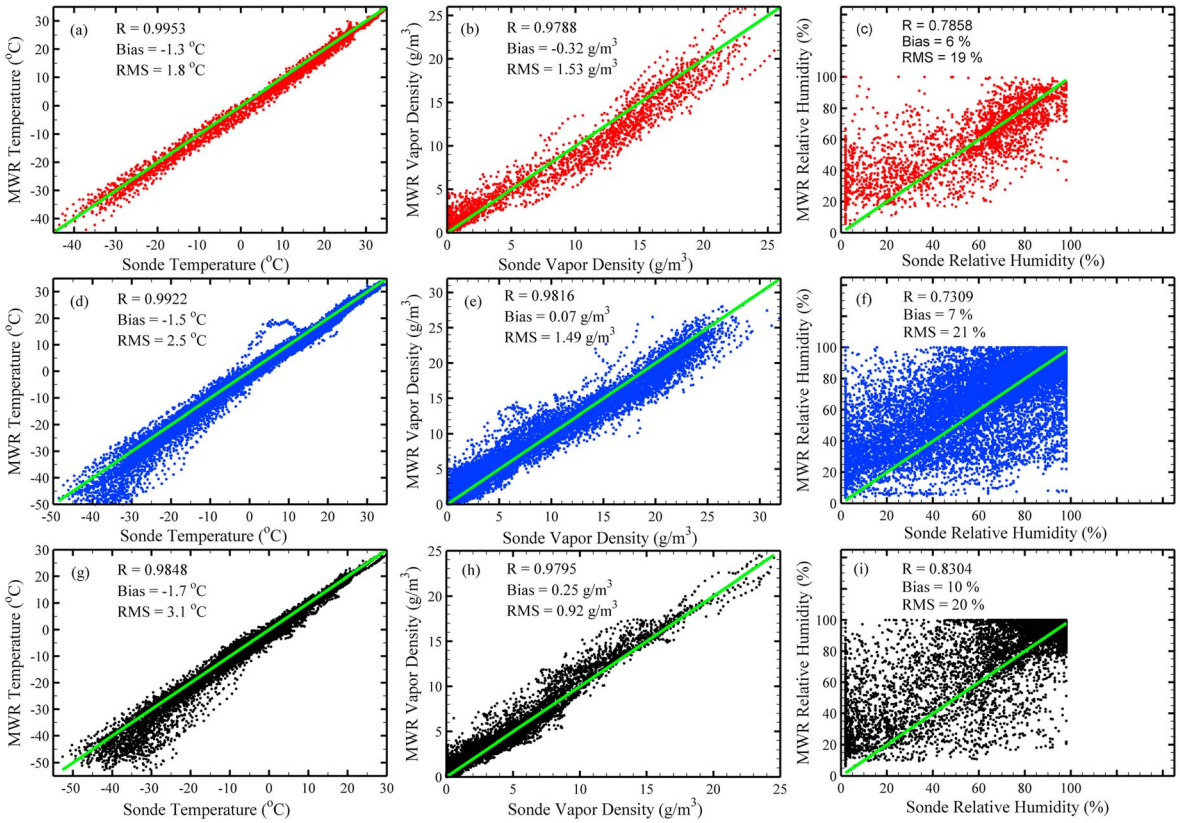

Figure 5. Scatterplots for MWR-retrieved (a, d, and g) temperature, (b, e, and h) vapor density, and (c, f, and i) relative humidity against radiosondes under low (Figures 5g–5i, black dots), middle (Figures 5d–5f, blue dots), and high (Figures 5a–5c, red dots) clouds. There are a total of 8062, 15,892, and 2726 samples under low, middle, and high clouds, respectively, from June 2010 to December 2013.

coefficient, bias, and RMS between clear and cloudy skies are primarily resulted from their corresponding wind speeds and drifting distances. As the radiosondes drift farther away from the ground-based MWR at higher levels, the differences between the MWR retrievals and radiosonde soundings become large because they are not measuring the same atmospheric parameter. The differences may be larger for atmospheric water vapor and RH for heterogeneous atmosphere at upper levels.

Table 1. Comparison of MWR Retrievals Against Radiosondes Under Clear and Cloudy Skies As Well As Low, Middle, and High Clouds[a]

Parameters	Sky Conditions	Number of Samples	Correlation Coefficient	Bias	RMS
Temperature	Clear	23,374	0.9885	−3.0°C	3.4°C
	Cloudy	44,080	0.9907	−1.5°C	2.7°C
	High cloud	2,726	0.9953	−1.3°C	1.8°C
	Middle cloud	15,892	0.9922	−1.5°C	2.5°C
	Low cloud	8,062	0.9848	−1.7°C	3.1°C
Vapor density	Clear	23,374	0.9387	−0.04 g/m^3	1.08 g/m^3
	Cloudy	44,080	0.9805	0.09 g/m^3	1.34 g/m^3
	High cloud	2,726	0.9788	−0.32 g/m^3	1.53 g/m^3
	Middle cloud	15,892	0.9816	0.07 g/m^3	1.49 g/m^3
	Low cloud	8,062	0.9795	0.25 g/m^3	0.92 g/m^3
Relative humidity	Clear	23,374	0.7045	8%	20%
	Cloudy	44,080	0.7653	8%	21%
	High cloud	2,726	0.7858	6%	19%
	Middle cloud	15,892	0.7309	7%	21%
	Low cloud	8,062	0.8304	10%	20%

[a]A total of 403 clear-sky and 760 cloudy-sky profiles has been selected from June 2010 to December 2013, and the selected profiles under low, middle, and high clouds are 139, 274, and 47, respectively. Each profile has 58 data points.

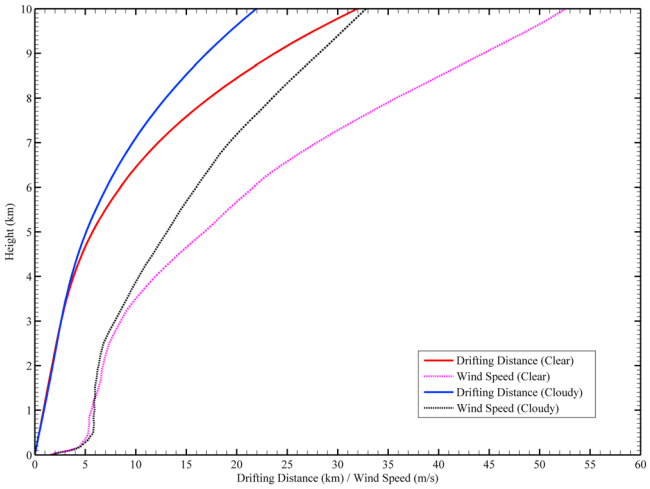

Figure 6. The variations of radiosonde balloon drifting distances and wind speeds along height based on a total 23,374 clear-sky samples and 44,080 cloudy samples.

4. Conclusions

The MWR-retrieved atmospheric temperature, vapor density, and relative humidity profiles under clear and cloudy skies have been compared with the collocated radiosonde sounding measurements at Wuhan from June 2010 to December 2013. Furthermore, the low, middle, and high clouds have been classified and compared with radiosonde measurements. A total of 403 profiles under clear sky and 760 profiles under cloudy sky have been selected in this study. Finally, we investigate the impact of wind speeds on the MWR retrievals. Based on the comprehensive study, we draw the following conclusions:

1. Based on the comparisons between the MWR retrievals and radiosonde sounding measurements, we draw the following three conclusions: (a) the temperature comparisons are better than the water vapor and RH ones due to more weighting functions used in MWR temperature retrievals and short drifting distance of radiosondes, (b) the comparisons at lower levels are better than those at upper levels because more weighting functions at lower levels; and (c) the cloudy comparisons are better than the clear-sky ones due to less solar heating on the radiosonde sensors and short drifting distance of radiosondes during cloudy than during clear sky. The decreased correlation coefficients and increased temperature biases and RMSs with height for both clear and cloudy skies are strongly associated with the increased wind speeds and drifted distances.
2. Three types of clouds (low, middle, and high) with 139, 274, and 47 profiles, respectively, are identified and compared with collocated radiosonde soundings to investigate the uncertainties of the MWR retrievals. For temperature comparisons, high cloud has the highest correlation coefficient and the lowest bias and RMS, but low cloud is in the opposite direction. For water vapor density comparisons, middle cloud has the highest correlation and the lowest bias, and high cloud has the lowest correlation coefficient and the largest bias and RMS.
3. Based on a total of 23,374 clear-sky samples and 44,080 cloudy samples, we conclude that both clear and cloudy wind speeds increase with heights, but clear-sky wind speeds increase much faster than cloudy ones above 4 km, and the radiosonde drifting distance is strongly associated with corresponding wind speed. For the impact of wind speeds on the MWR retrievals, we conclude that the decreased correlation coefficients and increased temperature biases and RMSs with height for both clear and cloudy skies are strongly associated with the increased wind speeds and drifted distances. The differences in correlation coefficient, bias, and RMS between clear and cloudy skies are primarily resulted from their corresponding wind speeds and drifting distances.

Acknowledgments

This work was supported by the National Natural Science Foundation of China (grants 41175016, 41375041, 41541037 and 41375057), and the National High Technology Research and Development Program ("863" Program) of China (grant 2012AA120902), and the open project of State Key Laboratory of Severe Weather, Chinese Academy of Meteorological Sciences (grant 2013LASW-A02). Xiquan Dong was partially supported by the National Basic Research Program of China (973 Program, 2013CB955803) at Beijing Normal University. Special thanks for Timothy Logan to read the manuscript and provide a lot of useful suggestions. The data used to produce results can be obtained from Guirong Xu (grxu@whihr.com.cn).

References

Bian, J., H. Chen, H. Vömel, Y. Duan, Y. Xuan, and D. Lü (2011), Intercomparison of humidity and temperature sensors: GTS1, Vaisala RS80, and CFH, *Adv. Atmos. Sci.*, *28*, 139–146.

Cadeddu, M. P., J. C. Liljegren, and D. D. Turner (2013), The atmospheric radiation measurement (ARM) program network of microwave radiometers: Instrumentation, data, and retrievals, *Atmos. Meas. Tech.*, *6*, 2359–2372.

Calheiros, A. J. P., and L. A. T. Machado (2014), Cloud and rain liquid water statistics in the CHUVA campaign, *Atmos. Res.*, *144*, 126–140.
Campos, E. F., R. Ware, P. Joe, and D. Hudak (2014), Monitoring water phase dynamics in winter clouds, *Atmos. Res.*, *147–148*, 86–100.
Chan, P. W. (2009), Performance and application of a multi-wavelength, ground-based microwave radiometer in intense convective weather, *Meteorol. Z.*, *18*, 253–265.
Chan, P. W., and K. K. Hon (2011), Application of ground-based, multi-channel microwave radiometer in the nowcasting of intense convective weather through instability indices of the atmosphere, *Meteorol. Z.*, *20*, 423–429.
Cimini, D., T. J. Hewison, L. Martin, J. Güldner, C. Gaffard, and F. Marzano (2006), Temperature and humidity profile retrievals from ground-based microwave radiometers during TUC, *Meteorol. Z.*, *15*, 45–56.
Cimini, D., E. Campos, R. Ware, S. Albers, G. Graziano, J. Oreamuno, P. Joe, S. Koch, S. Cober, and E. Westwater (2011), Thermodynamic atmospheric profiling during the 2010 Winter Olympics using ground-based microwave radiometry, *IEEE Trans. Geosci. Remote Sens.*, *49*, 4959–4969.
Cimini, D., F. De Angelis, J.-C. Dupont, S. Pal, and M. Haeffelin (2013), Mixing layer height retrievals by multichannel microwave radiometer observations, *Atmos. Meas. Tech.*, *6*, 4971–4998.
Clements, C. B., and A. J. Oliphant (2014), The California State University-Mobile Atmospheric Profiling System (CSU-MAPS): A facility for research and education in boundary-layer meteorology, *Bull. Am. Meteorol. Soc.*, doi:10.1175/BAMS-D-13-00179.1.
Dong, X., B. Xi, and P. Minnis (2006), A climatology of midlatitude continental clouds from ARM SGP site. Part II: Cloud fraction and surface radiative forcing, *J. Clim.*, *19*, 1765–1783.
Durre, I., R. S. Vose, and D. B. Wuertz (2008), Robust automated quality assurance of radiosonde temperatures, *J. Appl. Meteorol. Climatol.*, *47*, 2081–2095.
Güldner, J., and D. Spänkuch (2001), Remote sensing of the thermodynamic state of the atmospheric boundary layer by ground-based microwave radiometry, *J. Atmos. Oceanic Technol.*, *18*, 925–933.
Gultepe, I., et al. (2015), A review on ice fog measurements and monitoring, *Atmos. Res.*, *151*, 2–19.
Harikishan, G., B. Padmakumari, R. S. Maheskumar, G. Pandithurai, and Q. L. Min (2014), Macrophysical and microphysical properties of monsoon clouds over a rain shadow region in India from ground-based radiometric measurements, *J. Geophys. Res. Atmos.*, *119*, 4736–4749, doi:10.1002/2013JD020872.
Hewison, T. (2007), 1D-VAR retrievals of temperature and humidity profiles from a ground-based microwave radiometer, *IEEE Trans. Geosci. Remote Sens.*, *45*, 2163–2168.
Knupp, K., R. Ware, D. Cimini, F. Vandenberghe, J. Vivekanandan, E. Westwater, and T. Coleman (2009), Ground-based passive microwave profiling during dynamic weather conditions, *J. Atmos. Oceanic Technol.*, *26*, 1057–1073.
Liljegren, J. C., E. E. Clothiaux, G. G. Mace, S. Kato, and X. Dong (2001), A new retrieval for cloud liquid water path using a ground-based microwave radiometer and measurements of cloud temperature, *J. Geophys. Res.*, *106*, 14,485–14,500, doi:10.1029/2000JD900817.
Löhnert, U., S. Crewell, and C. Simmer (2004), An integrated approach towards retrieving physically consistent profiles of temperature, humidity, and cloud liquid water, *J. Appl. Meteorol.*, *43*(9), 1295–1307.
Madhulatha, A., M. Rajeevan, M. V. Ratnam, J. Bhate, and C. V. Naidu (2013), Nowcasting severe convective activity over southeast India using ground-based microwave radiometer observations, *J. Geophys. Res. Atmos.*, *118*, 1–13, doi:10.1029/2012JD018174.
Morris, V., C. Long, and D. Nelson (2006), Deployment of an infrared thermometer network at the Atmospheric Radiation Measurement Program Southern Great Plains Climate Research Facility, *Sixteenth Atmospheric Radiation (ARM) Science Team Meeting*, Proceedings. [Available at https://www.arm.gov/publications/proceedings/conf16/extended_abs/morris_vr.pdf.]
Raju, C. S., R. Renju, T. Antony, N. Mathew, and K. K. Moorthy (2013), Microwave radiometric observation of a waterspout over coastal Arabian Sea, *IEEE Trans. Geosci. Remote Sens.*, doi:10.1109/LGRS.2012.2229960.
Serke, D., et al. (2014), Supercooled liquid water content profiling case studies with a new vibrating wire sonde compared to a ground-based microwave radiometer, *Atmos. Res.*, *149*, 77–87.
Solheim, F. S., J. R. Godwin, E. R. Westwater, Y. Han, S. J. Keihm, K. Marsh, and R. Ware (1998), Radiometric profiling of temperature, water vapor, and cloud liquid water using various inversion methods, *Radio Sci.*, *33*, 393–404, doi:10.1029/97RS03656.
Spänkuch, D., J. Güldner, H. Steinhagen, and M. Bender (2011), Analysis of a drylin-like feature in northern Germany detected by ground-based microwave profiling, *Meteorol. Z.*, *20*, 409–421.
Starr, D. O., and S. H. Melfi (Eds) (1991), *The Role of Water Vapor in Climate: A Strategic Research Plan for the Proposed GEWEX Water Vapor Project (GVaP)*, *NASA Conf. Publ., CP-3120*, 50 pp. [Available at http://ntrs.nasa.gov/archive/nasa/casi.ntrs.nasa.gov/19910016242.pdf.]
Venkat Ratnam, M., Y. Durga Santhi, M. Rajeevan, and S. Vijaya Bhaskara Rao (2013), Diurnal variability of stability indices observed using radiosonde observations over a tropical station: Comparison with microwave radiometer measurements, *Atmos. Res.*, *124*, 21–33.
Vömel, H., H. Selkirk, L. Miloshevich, J. Valverde-Canossa, J. Valdes, E. Kyro, R. Kivi, W. Stolz, G. Peng, and J. Diaz (2007), Radiation dry bias of the Vaisala RS92 humidity sensor, *J. Atmos. Oceanic Technol.*, *24*, 953–963.
Ware, R., R. Carpenter, J. Güldner, J. Liljegren, T. Nehrkorn, F. Solheim, and F. Vandenberghe (2003), A multi-channel radiometric profiler of temperature, humidity and cloud liquid, *Radio Sci.*, *38*(4), 8079, doi:10.1029/2002RS002856.
Ware, R., D. Cimini, E. Campos, G. Giuliani, S. Albers, M. Nelson, S. E. Koch, P. Joe, and S. Cober (2013), Thermodynamic and liquid profiling during the 2010 Winter Olympics, *Atmos. Res.*, *132–133*, 278–290.
Xi, B., X. Dong, P. Minnis, and M. Khaiyer (2010), A 10-yr climatology of cloud cover and vertical distribution from both surface and GOES observations over DOE ARM SGP site, *J. Geophys. Res.*, *115*, D12124, doi:10.1029/2009JD012800.
Xie, Y., S. Koch, J. McGinley, S. Albers, P. Bieringer, M. Woflson, and M. Chan (2011), A space-time multiscale analysis system: A sequential variational analysis approach, *Mon. Weather Rev.*, *139*, 1224–1240.
Xu, G., R. Ware, W. Zhang, G. Feng, K. Liao, and Y. Liu (2014), Effect of off-zenith observations on reducing the impact of precipitation on ground-based microwave radiometer measurement accuracy, *Atmos. Res.*, *140*, 85–94.
Yoneyama, K., M. Fujita, N. Sato, M. Fujiwara, Y. Inai, and F. Hasebe (2008), Correct for radiation dry bias found in RS92 radiosonde data during the MISMO field experiment, *SOLA*, *4*, 13–16.